Laser-spot step-heating thermography to measure the thermal diffusivity of solids

A. Salazar*, M. Colom and A. Mendioroz

Departamento de Física Aplicada I, Escuela de Ingeniería de Bilbao, Universidad del País Vasco UPV/EHU, Plaza Ingeniero Torres Quevedo 1, 48013 Bilbao, Spain

*Corresponding author, E-mail address: agustin.salazar@ehu.es

ABSTRACT

In this work we show that laser-spot step-heating thermography allows measuring the thermal diffusivity of solids accurately. It consists in illuminating the sample surface with a continuous-wave focused laser spot and recording the time evolution of the surface temperature with an infrared camera. The inherent noise associated to time domain measurements is reduced by applying a very simple image processing procedure. The methodology has been tested on reference samples. Unlike laser spot lock-in (or pulsed) thermography, a step-heating thermography device can be easily put together combining a low-end laser and an entry level IR camera.

Keywords: infrared thermography, thermal diffusivity, laser spot, step-heating.

1. INTRODUCTION

Laser-spot infrared (IR) thermography, which consists in heating the sample under study with a focused laser beam and recording the surface temperature with an IR video camera, is a useful technique to measure the thermal diffusivity of solids. Regarding the temporal shape of the laser illumination two main configurations have been analyzed in the literature: (a) lock-in thermography, where the laser beam power is harmonically modulated at a given frequency and (b) pulsed thermography, where a brief laser pulse heats the sample. Both illumination schemes have been used to measure the thermal diffusivity of solids.

Laser-spot lock-in thermography takes advantage of the lock-in process to filter the signal: the higher the number of images that are processed, the lower the noise in the final amplitude and phase images. By analyzing the radial dependence of the amplitude and phase of the surface temperature, the thermal diffusivity of the sample can be obtained with a high accuracy. It has been widely used to measure the thermal diffusivity of bulk samples [1-11] and of thin films and monofilaments [12-23]. On the other hand, laser-spot pulsed thermography has also been proposed to measure the thermal diffusivity of solids [6, 24-28]. However, its use is less extended than the lock-in modality since high energy pulsed lasers are more expensive and dangerous than CW lasers and they can damage the specimen when they are tightly focused onto the sample surface. Besides these two temporal schemes, there is a third configuration, which is called step-heating thermography, where a CW laser is switched on at a given instant and the IR camera records the time evolution of the surface temperature. It has been used with flat illumination of the whole sample surface to image subsurface defects [29]. However, laser-spot step-heating has not been considered for measurements of the thermal diffusivity of solids. The reason why it has been underestimated for this purpose, although it may be easier to handle and less expensive than the other two ones, is probably due to the suspicion that it may produce too noisy signals for practical quantitative analysis.

The aim of this work is to evaluate whether laser-spot step-heating thermography provides accurate enough thermal diffusivity values for reliable implementation in both industrial environments and R&D departments. The first step is to solve the heat diffusion equation to find an analytical expression of the time evolution of the surface temperature. We will look for a solution as general as possible, i.e. valid for bulk samples and thin plates, opaque and highly transparent samples and taking into account heat losses by convection and radiation. The accuracy of the method will be tested by measuring the thermal diffusivity of a set of reference materials covering the range from thermal insulators to good thermal conductors. Finally, we will discuss on the viability of a low-cost device consisting of a low-end laser and an entry level IR camera.

2. THEORY

Let us consider a homogeneous and isotropic plate of thickness L, infinite in both OX and OY directions, illuminated by a continuous-wave (CW) laser beam of Gaussian profile whose power density has the following spatial distribution

$$P(r) = \frac{2P_o}{\pi a^2} e^{-\frac{2r^2}{a^2}}, \qquad (1)$$

where P_o is the laser power and a is its radius at $1/e^2$ of peak intensity. The laser is switched on at $t = 0$ so the time dependence of the power satisfies a Heaviside function: 0 for $t < 0$ and P_o for $t > 0$. The scheme of the illumination is shown in Fig. 1.

To obtain the time evolution of the sample temperature rise above the ambient $T(r,z,t)$ we have to solve the heat diffusion equation

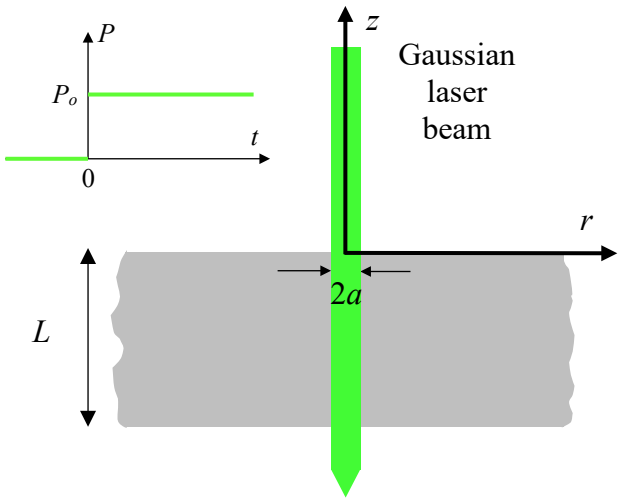

Figure 1. Cross section of a sample illuminated by a focused laser beam of radius *a*. The inset shows the time profile of the step-heating.

$$\nabla^2 T(r,z,t) - \frac{1}{D}\frac{\partial T(r,z,t)}{\partial t} = -\frac{Q(r,z,t)}{K}, \tag{2}$$

where Q is the energy absorbed per unit volume, and K and D are the thermal conductivity and diffusivity of the sample, respectively. If the laser beam is absorbed by the sample following the Beer-Lambert law, then $Q(r,z,t) = \eta P(r) u(t) \alpha e^{\alpha z}$, where $u(t)$ is the Heaviside unit step function and η is the laser power fraction absorbed by the sample. To solve Eq. (2) we perform a double transformation. First, a Laplace transform leading to

$$\nabla^2 \overline{T}(r,z,s) - \frac{s}{D}\overline{T}(r,z,s) = -\frac{1}{K}\eta P(r)\frac{1}{s}\alpha e^{\alpha z}, \tag{3}$$

where s is the conjugate variable of time and 1/s is the Laplace transform of $u(t)$. Then, due to the cylindrical symmetry of the problem, we apply a Hankel transform [30]

$$\frac{d^2\tilde{\overline{T}}(\delta,z,s)}{dz^2} - \beta^2 \tilde{\overline{T}}(\delta,z,s) = -\frac{1}{K}\eta\frac{P_o}{2\pi}e^{-\frac{(\delta a)^2}{8}}\frac{1}{s}\alpha e^{\alpha z}, \tag{4}$$

where $\beta^2 = s/D + \delta^2$, δ is the conjugate variable of r and $\frac{P_o}{2\pi}e^{-\frac{(\delta a)^2}{8}}$ is the Hankel transform of $P(r)$. The general solution of Eq. (4) is

$$\tilde{\overline{T}}(\delta,z,s) = Ae^{-\beta z} + Be^{\beta z} + Ce^{\alpha z}, \tag{5}$$

where $C = \frac{1}{K}\frac{\eta P_o}{2\pi}e^{-\frac{(\delta a)^2}{8}}\frac{1}{s}\frac{\alpha}{\beta^2 - \alpha^2}$. Depth-independent factors A and B will be obtained from the boundary conditions: the heat flux continuity at the sample surfaces, taking into account heat losses by convection and radiation

$$-K\left.\frac{dT}{dz}\right|_{z=0} = hT(z=0), \tag{6a}$$

$$-K\left.\frac{dT}{dz}\right|_{z=-L} = -hT(-L), \tag{6b}$$

where h is the linearized coefficient of heat losses. The double Laplace and Hankel transform of Eqs. (6) gives

$$-K\left.\frac{d\tilde{\tilde{T}}}{dz}\right|_{z=0} = h\tilde{\tilde{T}}(z=0) \tag{7a}$$

$$-K\left.\frac{d\tilde{\tilde{T}}}{dz}\right|_{z=-L} = -h\tilde{\tilde{T}}(z=-L). \tag{7b}$$

By substituting Eq. (5) into Eqs. (7), factors A and B are obtained, and therefore $\tilde{\tilde{T}}(\delta,z,s)$ writes

$$\tilde{\tilde{T}}(\delta,z,s) = C\left[\frac{Ee^{-\beta z}+Fe^{\beta z}}{(1+H)^2 e^{\beta L}-(1-H)^2 e^{-\beta L}}+e^{\alpha z}\right], \tag{8}$$

where

$$E = \left(\frac{\alpha}{\beta}-H\right)(1+H)e^{-\alpha L}-\left(\frac{\alpha}{\beta}+H\right)(1-H)e^{-\beta L}, \tag{9a}$$

$$F = \left(\frac{\alpha}{\beta}-H\right)(1-H)e^{-\alpha L}-\left(\frac{\alpha}{\beta}+H\right)(1+H)e^{\beta L}, \tag{9b}$$

and $H=\frac{h}{K\beta}$. The time evolution of the sample temperature is obtained by performing an inverse Hankel transform followed by an inverse Laplace transform. Unfortunately, there is no analytical solution for the inverse Laplace of Eq. (8). However, analytical expressions of the surface temperature can be obtained in three particular cases.

2.1. Opaque and thermally thick samples

An opaque sample verifies $\left(\alpha\to\infty,\ e^{-\alpha L}\approx 0\right)$. This means that the laser beam is absorbed at the sample surface. On the other hand, the thermal diffusion length in step-heating transient heat conduction problems is defined as $\mu=\sqrt{Dt}$ [31]. A thermally thick sample verifies $L >> \mu$ $\left(e^{-\beta L}\approx 0\right)$, indicating that heat does not reach the rear surface. Under these restrictions Eq. (8) reduces to

$$\tilde{\tilde{T}}(\delta,0,s) \approx \frac{1}{s}\frac{\eta P_o}{2\pi K}\frac{1}{\beta+\frac{h}{K}}e^{-\frac{(\delta a)^2}{8}}. \tag{10}$$

A double inverse Hankel and Laplace transform gives the temperature rise above the ambient of an opaque and thermally thick sample at the illuminated surface (z = 0), which can be measured by an IR camera

$$T(r,0,t) \approx \frac{\eta P_o}{2\pi K}\int_0^\infty \delta J_o(\delta r)e^{-\frac{(\delta a)^2}{8}}\times \tag{11}$$
$$\times\frac{\frac{h}{K}\left[e^{-Dt\left(\delta^2-\frac{h^2}{K^2}\right)}-1\right]-\frac{h}{K}e^{-Dt\left(\delta^2-\frac{h^2}{K^2}\right)}erf\left(\frac{h\sqrt{Dt}}{K}\right)+\delta erf\left(\delta\sqrt{Dt}\right)}{\delta^2-\frac{h^2}{K^2}}d\delta,$$

where J_o is the Bessel function of order zero and *erf* is the error function. Note that parameter h is always correlated to the thermal conductivity of the sample (h/K), indicating that the effect of heat losses increases for poor thermal conducting materials. In the case of adiabatic boundary conditions Eq. (10) reduces to

$$T(r,0,t) \approx \frac{\eta P_o}{2\pi K}\int_0^\infty J_o(\delta r)\, erf\left(\delta\sqrt{Dt}\right) e^{-\frac{(\delta a)^2}{8}}\, d\delta\,. \tag{12}$$

2.2. Opaque and thermally thin samples

A sample is thermally thin if it verifies $L << \mu$, so $e^{\pm\beta L} \approx 1 \pm \beta L$. Under this assumption Eq. (8) reduces to

$$\tilde{\tilde{T}}(\delta,s) \approx \frac{1}{s}\frac{\eta P_o}{2\pi KL}\frac{1}{\beta^2 + \frac{2h}{KL}} e^{-\frac{(\delta a)^2}{8}}, \tag{13}$$

which is independent of depth. The inverse Hankel and Laplace transforms give the temperature rise above the ambient

$$T(r,t) \approx \frac{\eta P_o}{2\pi KL}\int_0^\infty \delta J_o(\delta r)\frac{1-e^{-Dt\left(\delta^2+\frac{2h}{KL}\right)}}{\delta^2 + \frac{2h}{KL}} e^{-\frac{(\delta a)^2}{8}}\, d\delta\,. \tag{14}$$

Note that the thinner the sample the higher the effect of heat losses.

2.3. Highly transparent samples

In highly transparent samples ($\alpha \to 0$, $e^{-\alpha L} \approx 1$) Eq. (8) reduces to

$$\tilde{\tilde{T}}(\delta,s) \approx \frac{1}{s}\frac{\eta P_o}{2\pi K}\frac{\alpha}{\beta^2 + \frac{2h}{KL}} e^{-\frac{(\delta a)^2}{8}}, \tag{15}$$

whose double inverse Hankel and Laplace transform is

$$T(r,t) \approx \frac{\eta P_o \alpha}{2\pi K}\int_0^\infty \delta J_o(\delta r)\frac{1-e^{-Dt\left(\delta^2+\frac{2h}{KL}\right)}}{\delta^2 + \frac{2h}{KL}} e^{-\frac{(\delta a)^2}{8}}\, d\delta\,, \tag{16}$$

which is valid regardless of the sample thickness. Note that the last expression resembles the case of an opaque and thermally thin sample, Eq. (13), just replacing $1/L$ by α in the factor multiplying the integral.

Finally, let us note that Eqs. (14) and (16) which describe the temperature distributions in opaque thermally thin materials and highly transparent samples, respectively, are independent of the z coordinate, indicating that the temperature distribution at any inner plane parallel to the surface is identical. As a result, Eqs. (14) and (16) are also valid (except for a factor) to describe the distribution of the radiation emitted by samples that are semi-transparent in the IR bandwidth detected by the camera. On the contrary, Eq. (11) only describes the temperature at the surface of opaque and thermally thick materials. Therefore, Eq. (11) is only valid if, in addition to being opaque to the laser beam radiation, the material is also opaque to the IR radiation detected by the camera. However, this is not a significant limitation as a large number of materials are opaque to both, the visible radiation and IR region where IR cameras are sensitive.

3. NUMERICAL CALCULATIONS

3.1. Opaque and thermally thick samples

Following the theory developed in the section 2, next we use Eq. (11) to calculate temperature radial profiles of an opaque and thermally thick sample illuminated by a focused laser beam, which is switched on at $t = 0$. In Fig. 2a we show several temperature profiles for a polymeric sample (D = 0.2 mm^2/s, K = 0.4 Wm^{-1}K^{-1}) illuminated by a laser spot of radius a = 0.2 mm, from which it absorbs a power ηP_o = 10 mW. Three instants are considered (1, 2 and 5 s) and, for each, two heat losses coefficients are evaluated: $h = 0$ (black line) and h = 10 Wm^{-2}K^{-1} (red line). The former indicates adiabatic boundary conditions and the latter is a realistic h value at room temperature [18]. As can observed, as time goes by heat propagates at longer radial distances, while the temperature at the position of the laser spot remains almost unchanged. On the other hand, the influence of heat losses is negligible even though the calculations have been performed for a poor thermally conducting sample. Accordingly, we can conclude that for thermally thick samples the effect of heat losses can be neglected in room temperature experiments.

In Fig. 2b we analyze how the thermal diffusivity of the sample modifies the shape of the temperature profile. Calculations have been performed with a = 0.2 mm under adiabatic boundary conditions, i.e. using Eq. (12) for a material whose thermal diffusivity (D = 0.1 mm^2/s) is of the same order of magnitude as in Fig. 2a and for materials with thermal diffusivities one, two and three orders of magnitude higher. In Eq (12), the thermal conductivity is a factor outside the integral, so it does not modify the shape of the temperature profile. Accordingly, for a better comparison of the temperature profiles for different thermal diffusivity values, we have performed the calculations keeping the $\eta P_o/K$ factor fixed: $\eta P_o/K$ = 0.025 Km. The calculations in Fig. 2b correspond to t = 5 s. As can be seen, as the thermal diffusivity rises the temperature profiles become wider, which reveals the high sensitivity of these radial profiles to D. Note that we have plotted the profiles of ln(T) rather than the bare temperature profiles to enhance the temperature differences at long distances from the laser spot, which will be of interest to measure the thermal diffusivity accurately.

In summary, to obtain the thermal diffusivity of an opaque and thermally thick sample, Eq. (12) must be fitted to the experimental ln(T) profile obtained at a given time instant with two free parameters: $\eta P_o/K$ and D. In order to retrieve a more consistent diffusivity value, several radial profiles recorded at different time instants should be fitted simultaneously as will be shown in section 4.

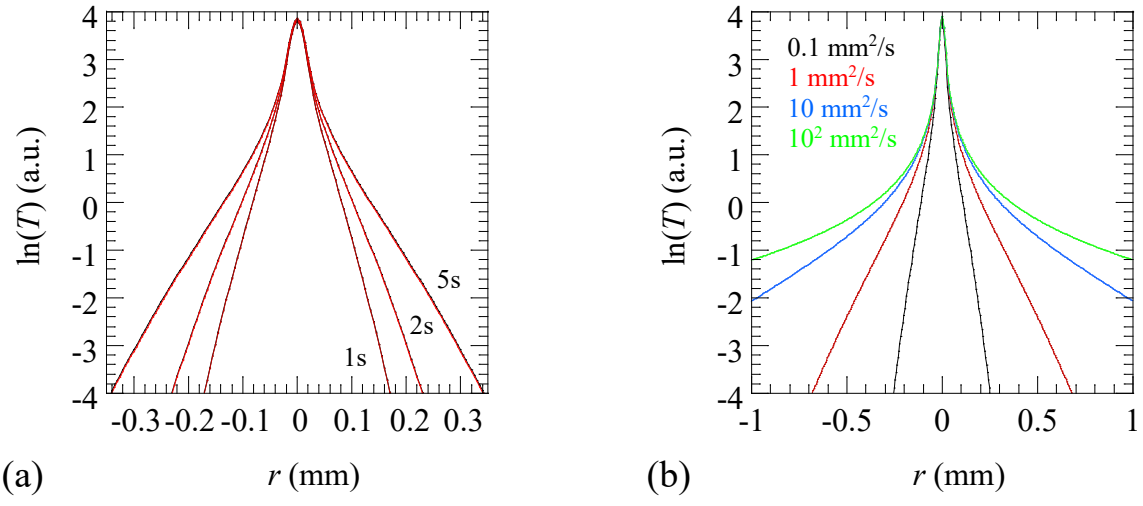

Figure 2. (a) Calculations of the temperature profiles (in logarithmic scale) for an opaque and thermally thick polymeric sample (D = 0.2 mm^2/s, K = 0.4 Wm^{-1}K^{-1}) with ηP_o = 10 mW and a = 0.2 mm. Three times are analyzed and for each time, two heat losses coefficients are considered: h = 0 (black line) and h = 10 Wm^{-2}K^{-1} (red line). (b) Calculations of the temperature profile for samples with different thermal diffusivities. Calculations have been performed for a = 0.2 mm, $\eta P_o/K$ = 0.025 Km, h = 0 and t = 5 s.

3.2. Opaque and thermally thin samples

In Fig. 3a we show the temperature profiles for the same opaque polymeric sample and experimental parameters as in Fig. 2a, but with a thickness L = 50 μm. Calculations have been performed using Eq. (14) for two instants (2 and 5 s) and for two heat losses coefficients: h = 0 (black line) and h = 10 Wm^{-2}K^{-1} (red line). Unlike for thermally thick samples, the effect of heat losses by convection and radiation cannot be neglected for thin plates. Accordingly, in order to measure the thermal diffusivity of thin samples Eq. (14) must be fitted to the experimental temperature profile, with three free parameters: $\eta P_o/K$, h/K and D. The first parameter controls the vertical position of the temperature profile while the shape of the curve is governed by the two last parameters. The question arises whether both parameters are independent or correlated. To assess this issue we calculate the sensitivity of ln(T) to each parameter, which is defined as

$$S_x = x\frac{\partial \ln(T)}{\partial x}, \quad x = D, h\,. \tag{17}$$

In Fig. 3b we show both sensitivities, S_D and S_h, for the same thermally thin material and experimental parameters as in Fig. 3a at t = 5 s. As can be observed, both sensitivities increase as we move away from the center of the laser spot. However, they are not correlated since both curves are not proportional. This means that for a given temperature profile only a couple (D,h) fits the experimental data.

In the case of highly transparent samples, the procedure is equivalent to opaque and thermally thin samples but using Eq. (16) instead of Eq. (14). Accordingly, the three free parameters to be fitted are: $\eta P_o \alpha/K$, h/K and D.

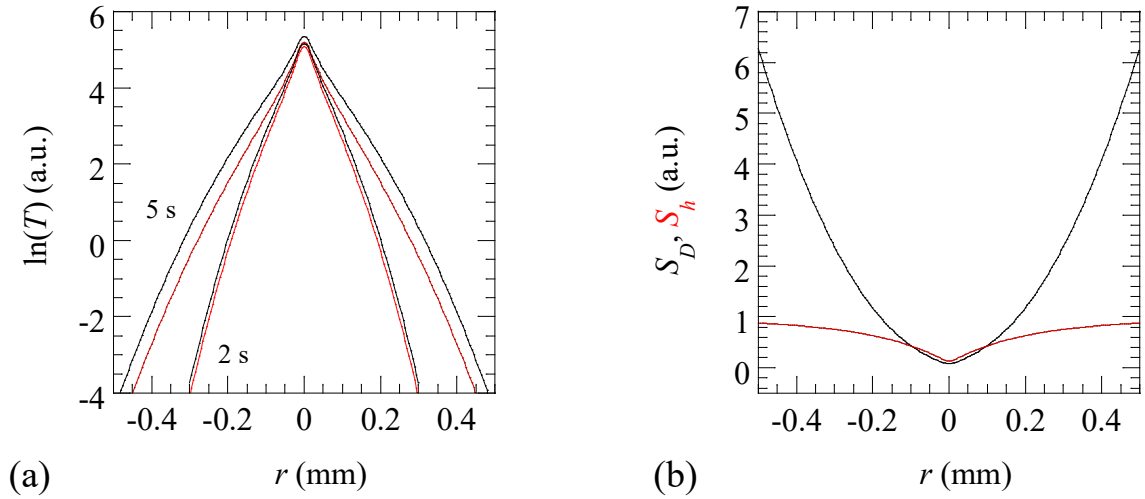

Figure 3. (a) The same as in Fig. 2a for a sample thickness L = 50 μm. Two times are analyzed and for each time, two heat losses coefficients are considered: h = 0 (black line) and h = 10

$Wm^{-2}K^{-1}$ (red line). (b) Calculation of the sensitivity of ln(T) to diffusivity, S_D, and to h/K, $S_{h/K}$, for the same sample at t = 5 s.

4. EXPERIMENTAL RESULTS AND DISCUSSION

In Fig. 4 we show the scheme of the laser-spot step-heating thermography setup. A CW laser (Coherent, Verdi V6, 532 nm, up to 6 W, beam diameter 2 mm) of Gaussian profile is focused onto the sample surface by a 10 cm focal length lens to a radius of about 200 μm. A Ge window, which is opaque to visible light but transparent to IR radiation, allows directing the laser beam perpendicularly to the sample. A mid-wave IR video camera (FLIR, SC 7500, 3-5 μm, 256×320 px, 450 frames/s, noise equivalent temperature difference (NETD) = 20 mK) records the surface temperature. The average of 10 frames recorded before the onset of the excitation is subtracted from the image sequence in order to obtain the temperature elevation above the ambient due to the excitation. In this way, we reduce the effect of emissivity heterogeneities and the Narcissus effect, which is very disturbing in the case of highly reflective samples such as metals and alloys. A macro lens produces a magnification ratio 1:1, i.e. each pixel of the detector senses the average temperature over a 30 μm square of the sample.

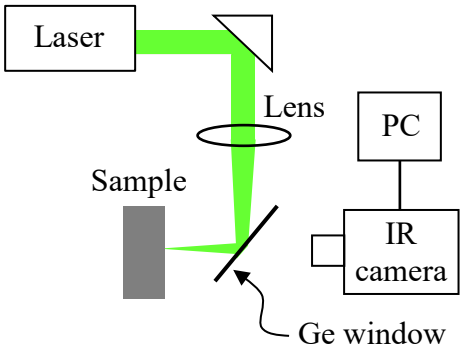

Figure 4. Scheme of the laser-spot step-heating thermography setup.

In Fig. 5 we show a sequence of thermograms (after background subtraction) corresponding to an opaque poly-ether-ether-ketone (PEEK) sample at four instants after the onset of the excitation: 1, 2, 5, 10 s. The laser power is P_o = 10 mW. As in the theoretical calculations, the thermograms show the natural logarithm of the temperature, ln(T), rather than the temperature itself, to better appreciate the low temperature regions. As predicted by the theory, heat propagates radially with time, but the temperature at the laser spot remains almost unchanged after the first second.

In Fig. 6 we plot by black dots the temperature profile along the vertical axis corresponding to the thermograms obtained at 1 and 5 s in Fig. 5. As it can be seen, the noise level is ln(T) ≈ -3, which corresponds to a temperature of 50 mK, not so far from the NETD of the camera. This noise level is higher than that obtained with laser spot lock-in thermography, which has been used to measure the thermal diffusivity of solids accurately. In lock-in thermography, the average noise level of the temperature amplitude image depends on the number of images that are processed in the lock-in analysis, N_{images}, as [32]

$$Noise = \frac{2}{\sqrt{N_{images}}} NETD\,. \tag{18}$$

This means that by collecting 10^3 images, the noise level is reduced down to 1 mK (Ln(T) ≈ -7), far below the NETD of the camera. To reduce the high noise level in step-heating thermography, we take advantage of the cylindrical symmetry of the thermograms to perform an average of the temperature along concentric circumferences around the laser spot. In this way, the longer the distances from the laser spot, where the noise is more pronounced, the larger the number of pixels that are averaged, leading to cleaner temperature profiles. The red dots in Fig. 6 correspond to such average profiles, showing that the noise level is reduced down to ln(T) ≈ -5, not far from that obtained in lock-in thermography.

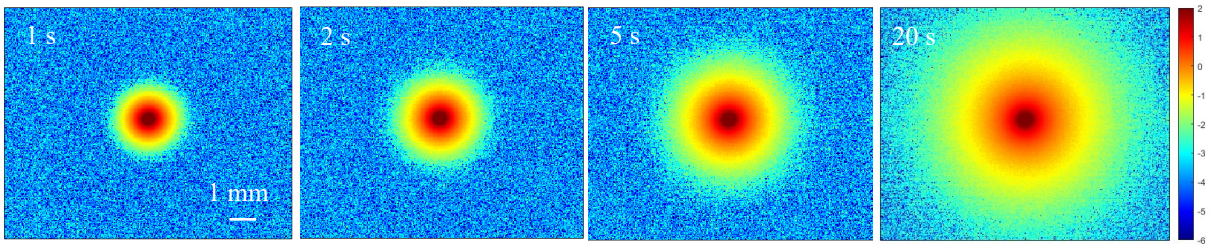

Figure 5. Sequence of thermograms of ln(T) obtained in a PEEK sample.

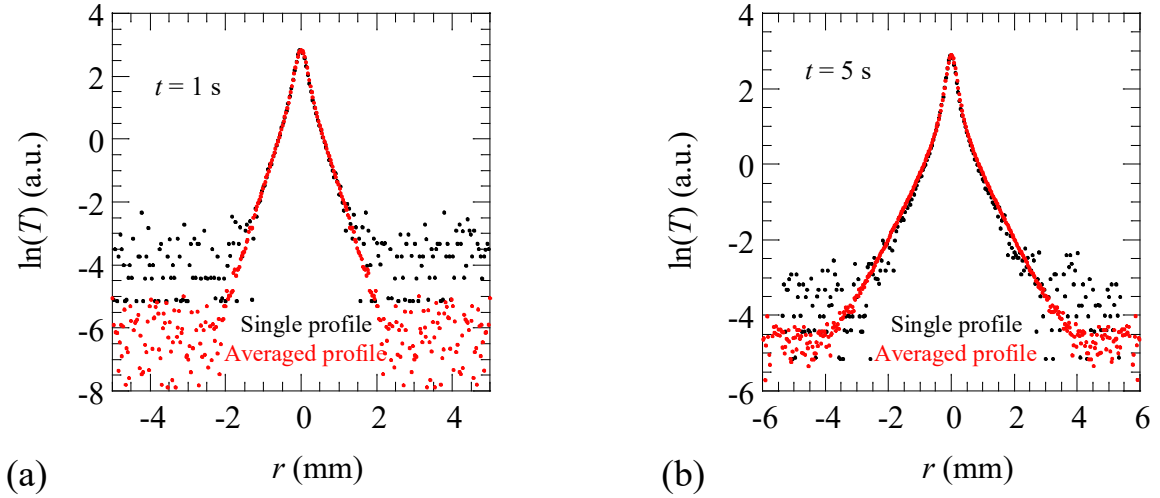

Figure 6. Comparison of single and averaged radial profiles of ln(T) obtained in a PEEK sample at two instants after the onset of the excitation.

To assess the validity of laser-spot step-heating thermography to measure the thermal diffusivity we have selected a series of calibrated materials covering a wide range of diffusivities from thermal insulators to good thermal conductors. A 4 mm thick PEEK sample, a 2 cm thick AISI-304 stainless steel, a 0.2 mm thick AISI-304 plate, a 6 mm thick vitreous carbon sample, a 9 mm thick graphite sample and a 2 mm thick light blue BK7 glass filter. As the PEEK sample is not completely opaque to visible light, a very thin graphite layer (about 3 μm thick) has been sprayed onto the surface.

In order to obtain reliable thermal diffusivity values we have fitted $T(r,t)$ to a set of temperature profiles obtained at several instants after the laser was switched on. In Fig. 7 we show the results for PEEK and graphite, which are opaque to the laser wavelength. On top, we plot by dots the average temperature profiles while the continuous lines are the best fits of Eq.

(12), which corresponds to opaque and thermally thick samples in the absence of heat losses. All the fittings in this work have been performed using a Levenberg-Marquardt algorithm. At the bottom, we plot the residuals, i.e. the difference between experimental and fitted values, to better assess the good quality of the fits. In the case of PEEK we have fitted temperature profiles from 1 s to 20 s. The fitted parameters are $\eta P_o/K = 2.383\times10^{-3}\pm3\times10^{-6}$ Km and $D = 0.207\pm0.001$ mm^2/s. For graphite we have fitted temperature profiles up to 0.4 s, since for longer times the sample is not thermally thick anymore. The fitted parameters are $\eta P_o/K = 0.2627\pm0.0006$ Km and $D = 64.9\pm0.9$ mm^2/s. As can be observed, the uncertainties of a single measurement are very low. By repeating the same measurement five times and at three different sample positions we obtained uncertainties in the range 3-5%, which are indicated in Table 1.

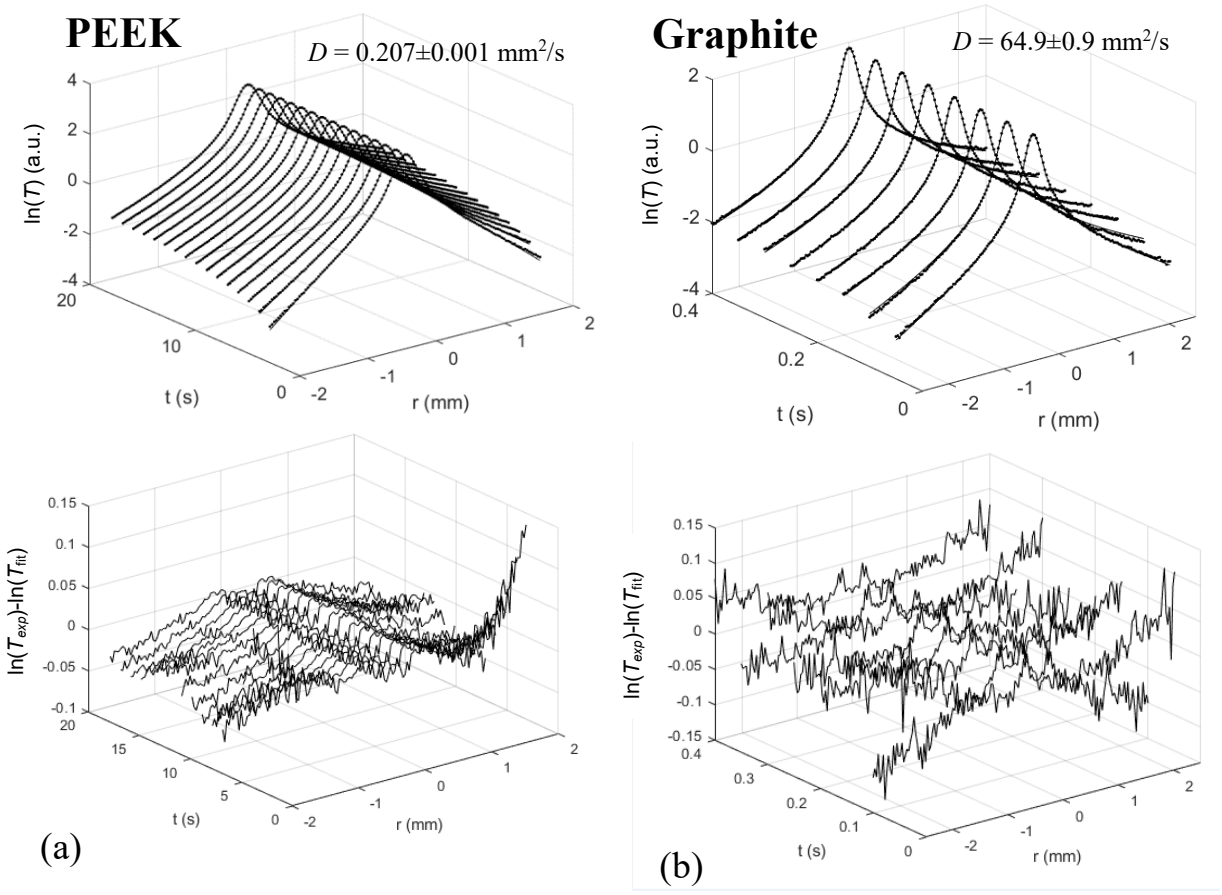

Figure 7. On top: simultaneous fittings of averaged profiles of ln(T) for two opaque and thermally thick samples. At the bottom: residuals are plotted to show the quality of the fittings.

In Fig. 8 we show the results for the 0.2 mm thick AISI-304 plate and for the light blue BK7 filter. The former is opaque and thermally thin and the latter is highly transparent. The experimental profiles corresponding to the AISI-304 plate have been fitted using Eq. (14). The fitted parameters are $\eta P_o/K = 0.0143\pm0.0001$ Km, $h/K = 1.1\pm0.2$ m^{-1} and $D = 3.85\pm0.06$ mm^2/s. The experimental profiles of the BK7 filter have fitted using Eq. (16). The fitted parameters are $\eta P_o\alpha/K = 1.686\times10^{-3}\pm2\times10^{-6}$ Km, $h/K = 5.8\pm0.5$ m^{-1} and $D = 0.433\pm0.001$ mm^2/s. As for the case of opaque and thermally thick samples, the uncertainties in the obtained parameters values are small. However, by repeating five for the each sample at three different surface locations we have obtained an uncertainty in D about 5%. The results for the six samples analyzed in this

work are summarized in Table 1, showing a good agreement with the literature values, together with an uncertainty about 5%.

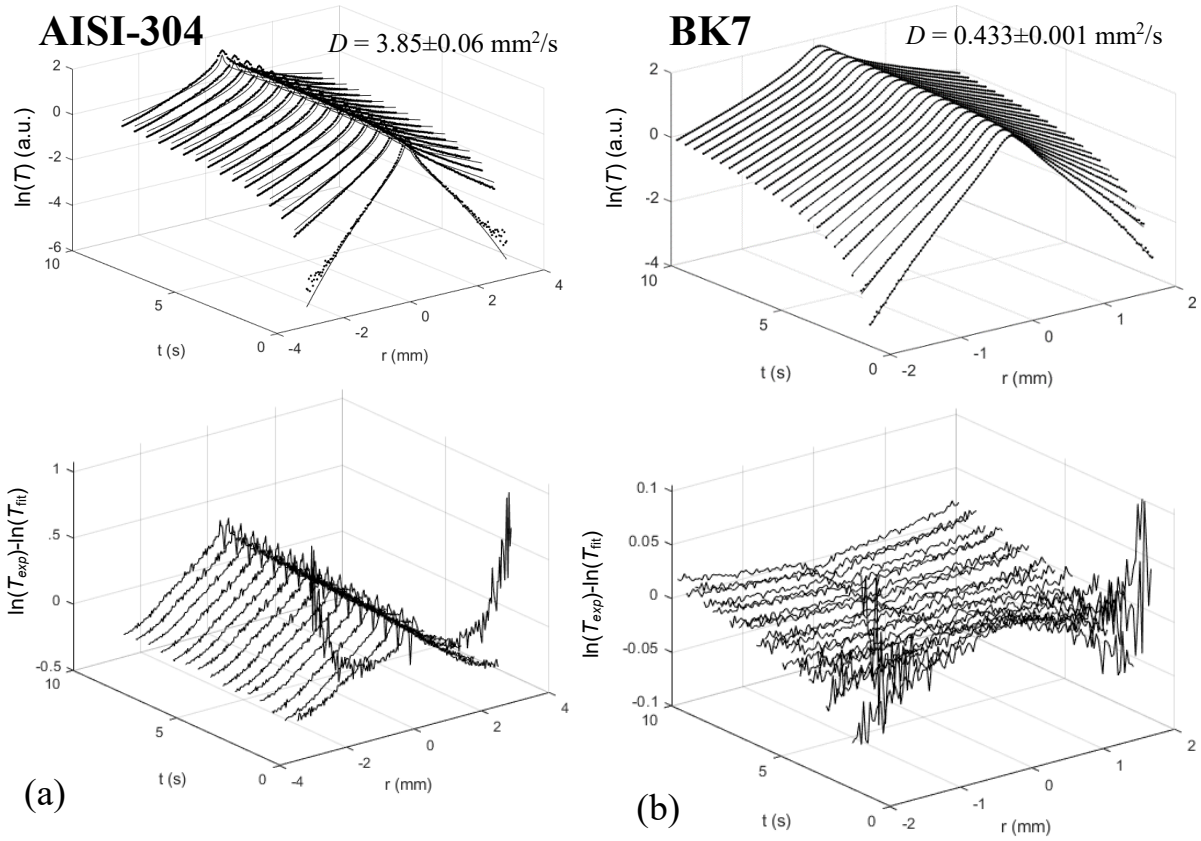

Figure 8. The same as Fig. 7 for an opaque and thermally thin sample (AISI-304, 0.2 mm thick) and for a very transparent sample (BK7 glass).

Table 1. Thermal diffusivity of the materials measured in this work.

Material	D (mm^2/s) This work	D (mm^2/s) Literature [34-38 27, 33-37]
PEEK	0.20 ± 0.01	0.20
AISI-304	3.9 ± 0.1	4.0
Glassy carbon	6.2 ± 0.2	6.0
Graphite	65 ± 2	60
AISI-304 (L = 0.2 mm)	3.9 ± 0.4	4.0
BK7 glass	0.44 ± 0.01	0.4-0.6

It has been demonstrated that, using a high-end CW laser and a scientific IR camera, laser-spot step-heating thermography is a valuable technique to measure the thermal diffusivity with high accuracy. This technique provides temperature profiles that are a bit noisier that those obtained with laser-spot lock-in thermography, but with the advantage of a simpler experimental setup.

In the remaining of this section, we will show that a high enough accuracy can be obtained using low-end lasers and entry-level IR cameras, thus proving that a low-cost equipment can be used to measure the thermal diffusivity accurately. On the one hand, we have used a laser delivering up to 6 W, but all measurements have been performed using powers in the range 10-500 mW that, according to nowadays technology, can be obtained with low-end lasers. On the other hand, inexpensive lasers do not feature Gaussian profile but a flat-top (top-hat) one. The spatial distribution of the power density of a flat-top laser of power P_o and radius a is given by

$$P(r) = \frac{P_o}{\pi a^2} \prod\left(\frac{r}{2a}\right), \tag{19}$$

where Π is the Heaviside pi function, whose value is 1 for $0 \le r \le a$ and 0 for $r > a$. Its Hankel transform is [30]

$$\tilde{P}(\delta) = \frac{P_o}{\pi} \frac{J_1(\delta a)}{\delta a}, \tag{20}$$

where J_1 is the Bessel function of order 1. Accordingly, to obtain the surface temperature of a sample illuminated by a top-hat laser, we just need to replace $0.5e^{-\frac{(\delta a)^2}{8}}$ by $\frac{J_1(\delta a)}{\delta a}$ in Eqs. (11), (12), (14) and (16). In Fig. 9 we show the comparison of the temperature profiles for a Gaussian laser beam and a top-hat one. Except at the position of the laser spot, where very scarce information on the sample diffusivity is available, the two temperature profiles are indistinguishable. Accordingly, the quality of the laser profile does not affect the validity of the method, as long as the spot is circular. It should be noted that, if the spot was elliptical, the temperature distribution would differ from the one presented in Section 2, as the solution should be calculated in the Fourier, rather than the Hankel space. Anyway, this does not represent a serious limitation since inexpensive laser diodes feature circular output with symmetric energy distributions. Then, the only requirement is to direct the laser beam perpendicular to the sample surface to guarantee a circular spot, which can be easily achieved by using a Ge window or a dichroic mirror.

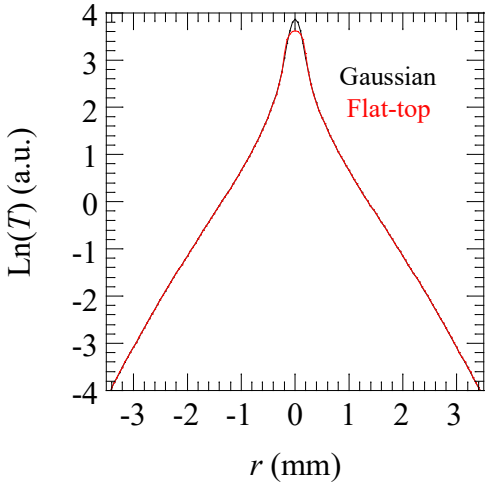

Figure 9. Calculations of the temperature profiles (in logarithmic scale) for an opaque and thermally thick polymeric sample (D = 0.2 mm^2/s, K = 0.4 Wm^{-1}K^{-1}) with ηP_o = 10 mW at t = 5 s, illuminated by a flat-top (red) and a Gaussian profile laser spot, both with a radius of a = 0.2 mm.

Regarding the IR camera we have used a medium level mid-wave IR camera with a NETD of 20 mK and a spatial resolution of 30 μm. Nowadays bolometer IR cameras feature NETD values of 50 mK, which does not represent a significant increase of the noise level. Regarding the spatial resolution, we have re-processed the temperature profiles, reducing the spatial resolution by performing the temperature average in squares of 5 px × 5 px to simulate a spatial resolution of 150 μm, which is the typical resolution of low-end IR cameras. In Fig. 10a we show the same temperature profile as in Fig. 6a, corresponding to a PEEK sample at t = 5 s. The black dots correspond to the full spatial resolution given by our IR camera (30 μm) while the red dots correspond to the reduced spatial resolution (150 μm). As can be observed, although the number of experimental data is reduced by a factor of five, the shape of the temperature profile remains unchanged. In Fig. 10b we show the fittings of the same series of temperature profiles as in Fig. 7a, but with the reduced spatial resolution. The quality of the fit is very good and the obtained thermal diffusivity value is the same as that obtained at full spatial resolution, within the experimental uncertainty. Note that the choice of PEEK to check the viability of using inexpensive equipment to measure the thermal diffusivity represents a "worst case scenario" in terms of spatial resolution, as in low diffusivity materials the temperature decays faster than in good conductors. Another key factor is the acquisition rate of the camera. In our camera this rate is 450 frames/s. This means that the uncertainty in the starting time of the illumination is 2 ms, whose influence in temperature profiles taken at times longer than 0.1 s is negligible. Low-end IR cameras have typical frame rates of 50 frames/s, introducing an uncertainty of 20 ms. To neglect this error, temperature profiles at times longer than 1 s must be used. This is not a great restriction, but introduces a lower limit to the lateral size of the sample, that must be greater than $2\mu = 2\sqrt{Dt}$, e.g. for a very good thermal conductor as Cu (D = 116 mm^2/s) and t = 4 the lateral size of the sample (length and width) must be longer than 5 cm.

In summary, we can conclude that thermal diffusivity of solids can be obtained accurately using a low-cost laser-spot step-heating device.

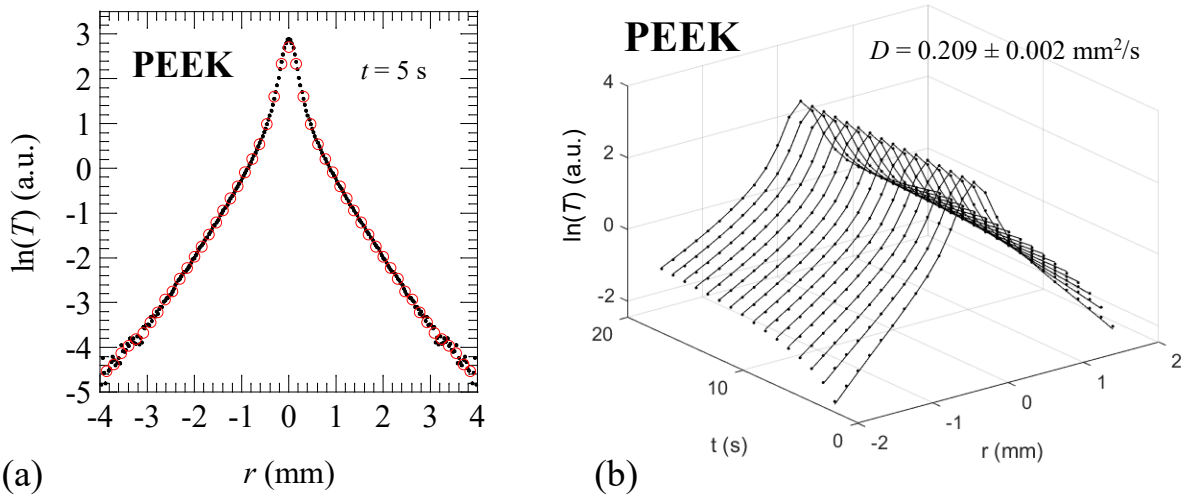

Figure 10. (a) Comparison of the radial profiles of ln(T) obtained at full spatial resolution (black dots) and at reduced resolution (red dots). (b) Simultaneous fittings of averaged profiles of ln(T) with reduced resolution.

5. SUMMARY AND CONCLUSIONS

We have shown that the thermal diffusivity of opaque and transparent isotropic materials can be measured using time domain IR thermography with laser-spot step-heating, with an accuracy similar to more sophisticated techniques such as laser-spot lock-in thermography. We have obtained semi-analytical expressions for the evolution of the surface temperature distribution when the material is illuminated by a CW laser spot, for a variety of material properties and sample configurations: opaque, transparent, thick and thin. We have analyzed the effect of heat losses by convection and radiation. The calculations show that the effect of heat losses is negligible in thick specimens, but needs to be considered if the sample is thin, especially in poor thermal conductors. The proposed methodology is based on fitting the theoretical temperature expression to radial temperature profiles. In order to gain consistency and accuracy, the noise in the radial profiles is reduced by averaging the temperature in circles concentric with the excitation and several averaged profiles obtained at different instants are fitted simultaneously. The averaging procedure is simpler than performing a lock-in analysis, both in terms of image processing and of the equipment needed, since no chopper or acousto-optic modulator is required in the set-up. The results show that the thermal diffusivity of materials ranging from good thermal conductors to thermal insulators, including thick and thin samples and semitransparent specimens can be measured with this technique with high accuracy and precision better than 5%. It has also been shown that inexpensive lasers and IR cameras can be used to build a low-cost laser-spot step-heating IR setup that enables accurate measurements of thermal diffusivity. If compared with a home-made classical flash system built with flash lamps, this system requires lower input energy and is easier to shield to prevent eye damage. In comparison with flash systems with laser excitation, pulsed lasers are significantly more expensive than laser diodes. Additionally, this methodology only needs one side access, which is interesting for assembled parts. As a summary, the proposed low-cost setup does not require sophisticated data processing and can be easily built and operated by non-specialized personnel in industrial environments.

Acknowledgments

This work has been supported by Ministerio de Ciencia e Innovación (PID2019-104347RB-I00, AEI/FEDER, UE), by Gobierno Vasco (PIBA 2018-15) and by Universidad del País Vasco UPV/EHU (GIU19/058).

REFERENCES

[1] L. Fabbri, P. Fenici, Three-dimensional photothermal radiometry for the determination of the thermal diffusivity of solids, Rev. Sci. Instrum. **66**, 3593 (1995).
[2] J.-C. Krapez, G. Gardette, Characterization of anisotropic materials by steady-state and modulated thermal ellipsometry, High Temp. High Press. **30**, 567 (1998).
[3] J.F. Bisson, D. Fournier, Influence of diffraction on low thermal diffusivity measurements with infrared photothermal microscopy, J. Appl. Phys. **83**, 1036 (1998).
[4] J.F. Bisson and D. Fournier, The coupled influence of sample heating and diffraction on thermal diffusivity estimate with infrared photothermal microscopy, J. Appl. Phys. **84**, 38 (1998).
[5] H.G. Walther and T. Kitzing, Systematic errors of locally resolved photothermal radiometry measurements, J. Appl. Phys. **84**, 1163 (1998).
[6] F. Cernuschi, A. Russo, L. Lorenzoni, A. Figari, In-plane thermal diffusivity evaluation by infrared thermography, Rev. Sci. Instrum. **72**, 3988 (2001).
[7] S. Paoloni and D. Fournier, Spectral dependence of signal distortions in spatially resolved photothermal radiometry, J. Appl. Phys. **92**, 5950 (2002).
[8] S. Paoloni and D. Fournier, Semi-empirical approach for the analysis of infrared photothermal microscopy, J. Appl. Phys. **92**, 5955 (2002).
[9] C. Boué and D. Fournier, New set-up to measure the thermal diffusivity with an infrared camera, J. Phys. IV France **125**, 101-104 (2005).
[10] L. Perez and L. Autrique, Robust determination of thermal diffusivity values from periodic heating data, Inverse problems **25**, 045011 (2009).
[11] T. Ishizaki and H. Nagano, Measurement of 3D thermal diffusivity distribution with lock-in thermography and application for high thermal conductivity CFRPs, Infrared Phys. Technol. **99**, 248-256 (2019).
[12] C.S. Welch, D.M. Heath, W.P. Winfree, Remote measurement of in-plane diffusivity components in plates, J. Appl. Phys. **61**, 895 (1987).
[13] B. Zhang and R. E. Imhof, Theoretical analysis of the surface thermal wave technique for measuring the thermal diffusivity of thin slabs, Appl. Phys. A, **62**, 323 (1996).
[14] M. Oksanen, R. Scholz and L. Fabbri, On the longitudinal thermal diffusivity of SiC-based fibres, J. Mat. Sci. Lett. **16**, 1092-1094 (1997).
[15] H. Kato, T. Baba and M. Okaji, Anisotropic thermal diffusivity measurements by a new laser-spot-heating technique, Meas. Sci. Technol. **12**, 2074-2080 (2001).
[16] A. Wolf, P. Pohl and R. Brendel, Thermophysical analysis of thin films by lock-in thermography, J. Appl. Phys. **96**, 6306-6312 (2004).
[17] C. Pradere, J.M. Goyhénèche, J.C. Batsale, S. Dilhaire and R. Pailler, Thermal diffusivity measurements on a single fiber with microscale diameter at very high temperature, Int. J. Therm. Sci. **45**, 443-451 (2006).
[18] A. Salazar, A. Mendioroz and R. Fuente, The strong influence of heat losses on the accurate measurement of thermal diffusivity using lock-in thermography, Appl. Phys. Lett. **95**, 121905 (2009).
[19] A. Mendioroz, R. Fuente-Dacal, E. Apiñaniz and A. Salazar, Thermal diffusivity measurements of thin plates and filaments using lock-in thermography, Rev. Sci. Instrum. **80**, 074904 (2009).
[20] A. Salazar, A. Mendioroz, R. Fuente and R. Celorrio, Accurate measurements of the thermal diffusivity of thin filaments by lock-in thermography, J. Appl. Phys. **107**, 043508 (2010).
[21] P.W. Nolte, T. Malvisalo, F. Wagner and S. Schweizer, Thermal diffusivity of metals determined by lock-in thermography, QIRT J. **14**, 218-225 (2017).

[22] A. Philipp, N.W. Pech-May, B.A.F. Kopera, A.M. Lechner, S. Rosenfeldt and M. Retsch, Direct measurement of the in-plane thermal diffusivity of semitransparent thin films by lock-in thermography: an extension of the slopes method, Anal. Chem. **91**, 8476-8483 (2019).
[23] J. Hahn, T. Reid and A. Marconnet, Infrared microscopy enhanced Angström's method for thermal diffusivity of polymer monofilaments and films, J. of Heat Transfer **141**, 081601 (2019).
[24] C.L. Choy, G.W. Yang and Y.W. Wong, Thermal diffusivity of polymer films by pulsed photothermal radiometry, J. Polym. Sci. B: Polym. Phys. **35**, 1621-1631 (1997).
[25] P. Bison, F. Cernuschi and S. Capelli, A thermographic technique for the simultaneous estimation of in-plane and in-depth thermal diffusivities of TBCs, Surface & Coating Technology **205**, 3128 (2011).
[26] H. Dong, B. Zheng and F. Chen, Infrared sequence transformation technique for in situ measurement of thermal diffusivity and monitoring of thermal diffusion, Infrared Phys. Technol. **73**, 130-140 (2015).
[27] N. W. Pech-May, A. Mendioroz and A. Salazar, Simultaneous measurement of the in-plane and in-depth thermal diffusivity of solids using pulsed infrared thermography with focused illumination, NDT&E Int. **77**, 28-34 (2016).
[28] L. Gaverina, A. Sommier, J. L. Battaglia, J. C. Batsale, C. Pradere, Pulsed Flying Spot Elliptic method for the estimation of the thermal diffusivity field of orthotropic materials, International Journal of Thermal Sciences, **125**, 142-148 (2018).
[29] R. Osiander and J.W.M. Spicer, Time-resolved infrared radiometry with step heating. A review, Rev. Gén. Therm. **37**, 680-692 (1998).
[30] R.N. Bracewell, The Fourier transform and its applications, 2nd edition (McGraw-Hill, New York, 1986), p. 244.
[31] A. Salazar, A. Oleaga and A Mendioroz, How far and fast does heat propagate?, Lat. Am. J. Phys. Educ. 13, 2307 (2019).
[32] O. Breitenstein and M. Langenkamp, Lock-in Thermography, Springer, Berlin (2003), p. 32.
[33] Y.A. Çengel, Heat Transfer: A practical Approach (McGraw-Hill, Boston, 2003).
[34] D.P. Almond and P.M. Patel, Photothermal Science and Techniques (Chapman & Hall, London, 1996), p. 16.
[35] See the Goodfellow catalogue in http://www.goodfellow.com for information on PEEK, AISI-304 and glassy carbon.
[36] L.R. Touloukian, R.W. Powell, C.Y. Ho, and M.C. Nicolasu, *Thermal Diffusivity* (IFI/Plenum, New York, 1973).
[37] M. Colom, A. Bedoya, A. Mendioroz and A. Salazar, Measuring the in-plane thermal diffusivity of moving samples using laser spot lock-in thermography, Int. J. Therm. Sci **151**, 106277 (2020).